Adaptive Main-Module Based Partial Power Processing for Wide-Range Operation of Current-Source Driven Modular MVDC

Zhijian Fang, *Member, IEEE,* Chi Zhang, *Student Member, IEEE,* Jinbo Zhao, Han Fu, Chunyu Ye, and Zhicong Huang, *Senior Member, IEEE*

***Abstract*—Constant current (CC) is widely employed in submarine observatory systems to transmit power over several thousand kilometers to the seabed, due to its robustness against cable impedance and short-circuit faults. Given the low current required to minimize transmission losses, a current-source-driven modular medium-voltage DC/DC converter (MVDC) is necessary to convert CC to constant voltage (CV) for powering the observatory equipment. However, this conversion faces challenges related to achieving a high voltage transfer ratio while maintaining efficiency over a wide load range. In this paper, an adaptive main-module-based partial power processing (PPP) approach is presented for the current-source driven modular MVDC. Unlike traditional strategies, where each module has the same droop characteristics, leading to a narrow voltage gain range and low efficiency under light load conditions, the proposed method features voltage-current droop curves that are different for each module and can be continuously arranged. The main module can be adaptive set to operate or bypass depending on the load condition, enabling a wide voltage gain range from 0 to the rated value, while maintaining high efficiency under light load conditions. Moreover, all modules can function flexibly, either as compensation or as main units, ensuring high redundancy. Finally, a CC-to-CV prototype consisting of four modules with $1\ A$ input current, 0 to $1.5\ kV$ input voltage and $375\ V/1.5\ kW$ output, is built to validate the proposed approach.**

***Index Terms*—submarine power supply, constant current, constant voltage, modular DC/DC converter, imbalance control.**

I. Introduction

CABLED submarine observatory system is emerging as the primary method for ocean observation, owing to its remarkable features of long-term, real-time, and in-situ monitoring [1]–[3]. To transmit power over several thousand kilometers to the seabed for submarine observation equipment, constant current (CC) is employed in the submarine power supply grid, due to its robustness against cable impedance and short circuit faults [4], [5]. Unlike the air with high dielectric properties, electric conductivity of seawater is very high up to $4.5S/m$, resulting into frequently short faults. In the CC system, the power supply from the source to the fault point can be maintained, obtaining high reliability. To minimize transmission losses, the current in the CC distribution system is typically kept low, often just several amperes, while the voltage is raised to several kilovolts (kV) to meet the power requirements of several kilowatts (kW) [6], [7]. Consequently, a current-source driven medium-voltage DC/DC converter (MVDC) is required to transfer the low constant current to constant voltage (CV) for the submarine observation equipments.

In the current-source driven applications, the input voltage could vary from 0 to the rated value resulting into a wide voltage range challenging the current-source driven converters. To address this issue, multiple Zener diodes are commonly employed to transfer CC to CV in the S-NET [8], owing to their simple architecture and high reliability. However, their power capacity is limited, making them unsuitable for meeting the high power demands of the undersea observation networks. To overcome this limitation, a multi-module parallel active resistance regulator scheme is proposed in Japan's DONET and DONET2 observation systems [9], [10], enabling high-power operation. However, this approach relies on passive resistance for output voltage regulation, leading to significant power losses. Power semiconductor switches are then used in current-source-driven DC/DC converters, such as the push-pull circuit, implemented in Chinese N-NET observation system [11]–[13], but the switching losses are introduced.

Alternatively, the series resonant converter proposed in [14] enables soft switching for higher efficiency, but it only provides controlled-current output. To achieve voltage regulation, an LCL-T resonant converter was proposed in [15], offering a load-independent CV feature along with soft switching. However, this method lacks robustness and requires precise parameter design. Then many resonant tank design methods have been studied and already been used in many industrial applications [16], [17]. But the power features of these methods are sensitive to the resonant tank. The variations of the parameters could worsen the performance. Unfortunately,

Manuscript received 28 March 2025, revised 10 July 2025, accepted 22 August 2025. This work is supported by the Key Research and Development Program of Hubei Province under Grant 2023BAB082, the Guangzhou Municipal Science and Technology Bureau under Grant 2025A04J7064, and the Science and Technology Planning Project of Guangdong Province under Grant 2023B0909050007. (Corresponding author: Zhicong Huang)

Z. Fang, C. Zhang, and C. Ye are with the Hubei Key Laboratory of Advanced Control and Intelligent Automation for Complex Systems, Engineering Research Center of Intelligent Technology for Geo-Exploration, Ministry of Education and the School of Automation, China University of Geosciences, Wuhan 430074, China (e-mail: fangzj@cug.edu.cn; chi_zhang@cug.edu.cn; yechunyu@cug.edu.cn).

J. Zhao is with Wuhan Maritime Communication Research Institution, Wuhan,430074, China (e-mail: zhaojinbo@hust.edu.cn).

H. Fu is with the School of Electrical and Electronic Information Engineering, Hubei Polytechnic University (HBPU), Huangshi 435000, China (e-mail: fuhan@hbpu.edu.cn).

Z. Huang is with the Shien-Ming Wu School of Intelligent Engineering, South China University of Technology, Guangzhou, 510006, China (e-mail: zhiconghuang@scut.edu.cn).

the equipments in the submarine need failure-free operate up to 20-25 years [18] requiring high robustness. Furthermore, all these approaches are constrained by high voltage stress, limiting their power capacities to only tens or hundreds of watts.

To address the high-power challenge, an input-series output-parallel (ISOP) modular structure, capable of achieving several kilowatts, has been employed, as demonstrated in the North American Pluto submarine observatory system. However, challenges related to multi-module controller design must still be addressed. In the Pluto submarine observatory system, a multi-module centralized synchronous control scheme is adopted, where all modules receive the same control signals from a central controller [19], [20]. While this approach is straightforward to implement, it requires high consistency among modules, which reduces system robustness. To overcome this limitation, [21]–[23]propose an average voltage control scheme for series-connected modules, supplemented by a voltage balance controller to equalize input voltage and power distribution, thereby mitigating the impact of module inconsistencies. However, due to the real-time module voltage communication the flexibility of these centralized control methods is limited. To address this issue, an adaptive droop control is added to regulate the voltage without extra communications [24]. But the inter-module coupling worsens the stability. A novel voltage balancing control strategy [25] is proposed to decouple the modular input voltage. But the extra PI controllers increase computational complexity and sacrifice the response speed of the system. To enhance system flexibility and reliability, decentralized control methods have been proposed [26]–[30]. But the control complexity is increased. Droop resistance adaptation is used realizing communication-free distributed control yet suffers from low accuracy [31]. Linear active disturbance rejection control (LADRC) is proposed to address this issue [32]. While these methods improve overall system robustness, the system efficiency remains limited, as all modules operate in the same state, leading to lower efficiency over a wide operating range.

The concept of partial power processing(PPP) has received more attention recently due to its excellent advantages of high efficiency over wide range [33], [34]. Only a small fraction of the total power is handled by the compensation module (CM) through active control, while the main power flow in the main module (MM) is not actively regulated or processed by control. Such that, High efficiency can be maintained in the MMs. However, the output voltage is also up to the CM, limiting the converter gain range. A hybrid control is proposed, where phase-shift controlled DAB is applied at high input voltage while the PFM-controlled resonant converter is utilized at low input voltage [35]. The gain range is extended but resulting into poor performance due to the controller switching. Then a two-stage PPP is proposed [36], [37] achieving wide voltage regulation range. Additional, limiting by the semiconductor devices, the voltages of all these converters are small, unable to be applied to medium voltage system.

Modular PPP, where several converters are series connected, is proposed for the medium voltage applications [38], [39]. The main power is transmitted by resonant converter operating at resonance frequency in the MM [40], [41]. To improve the efficiency, a switched-capacitor converter with P^4SFB is published in [42], reducing the current stress. In [43], the number of CM is increased to extend voltage range. However, the voltage range is still limited by the CMs in all these methods, which cannot adjust the extreme wide voltage range from 0 to the rated value in the current-source driven MVDC applications.

In this paper, an adaptive main-module based PPP strategy is proposed for current-source modular MVDC in submarine power supply system. The voltage-current droop curves of each module are different and continuously arranged for the modular input-series-output-parallel(ISOP) structure. There is only one module of which the V-I droop curve corsses the load curve. It is used to process the partial power, named as CM. The modules, curves above the load curve, are not actively regulated or processed working at the full power point delivering the main power defined as the MMs. While, the modules, curves below the load curve, are switched off regarded as redundant modules. Then the module converting the main power can be auto smoothly set to operate or bypass according to the load, achieving wide voltage gain range from 0 to the rated value and high efficiency especially in light load. Moreover, all modules can work freely as the compensation one or the main ones. High reliability can be obtained.

The comparison between the proposed method and traditional methods is presented in Table I. The main contributions of the proposed method are summarized as follows.

1) Wide input voltage range. The main module can be adaptive set to operate or bypass depending on the load condition, enabling a wide voltage gain range.
2) High efficiency over wide range. In the whole conditions, the MM could always operate at full load achieving the maximum efficiency obtaining high efficiency.
3) High reliability. Each module can automatically switch among MM, CM and bypassed modes. The reliability is increased exponentially according to the modules number.

The rest of this paper is organized as follows. Section II details the principle of proposed method. Section III analyzes the implement of adaptive main-module based PPP. Section IV discusses the performance of multi-module converter system. Experimental results validating the proposed method are provided in Section V. Finally, Section VI concludes this paper.

II. Conceptual Comparison of the Conventional Compensation Module based and the Proposed Main Module based Partial Power Processing

A. Topology and Modulation

The topology of current-source driven MVDC is given in Fig. 1. The input serial output parallel modular structure is used to adjust the input medium voltage and equalize the output current. Each module consists of a front shunt regulator (SR) and an end LLC resonant converter. The shunt regulator features a MOSFET Q_i (i denotes the module number) connected in parallel with the input side, and diode D_i placed between Q_i and bus capacitor C_cbi, providing the DC bus

TABLE I
COMPARISON OF MODULATION SCHEMES FOR BSRC

Power supply	Control method	Delivered power	Input voltage range	Efficiency of 30% load	Efficiency of 60% load	Efficiency of 100% load	Redundancy
Current-source driven [12] [13]	Centralized control	720W	0-800V	60%	80%	90%	Middle
Current-source driven [11]	Average voltage control	400W	0-460V	40%	None	None	Middle
Voltage-source driven [22]	Average voltage control	400W	400V	72%	80%	82%	Low
Voltage-source driven [29]	Decentralized control	100W	700-1000V	78%	87%	92%	High
Voltage-source driven [30]	Decentralized control	125W	1000V	67%	75%	77%	High
Voltage-source driven [39]	Modular PPP	600W	210V	87%	91.5%	91%	Low
Voltage-source driven [40]	Modular PPP@SRC	500W	220V	85%	93%	92%	Low
Current-source driven	Proposed method	1500W	0-1630V	91%	91%	92%	High

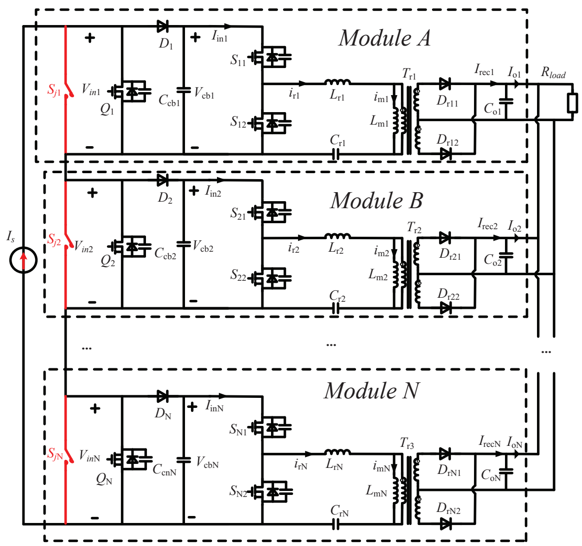

Fig. 1. Structure of current-source driven MVDC.

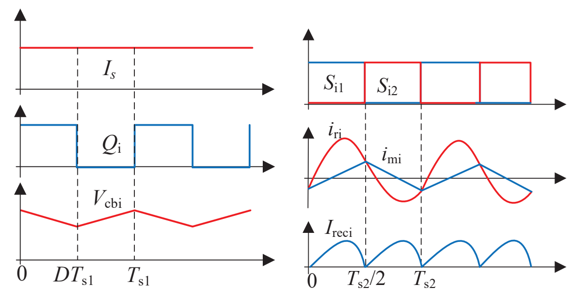

(a) Shunt regulator. (b) *LLC* converter.

Fig. 2. Waveforms of single CC-to-CV module.

voltage $V_{\rm cbi}$. The LLC resonant converter, cascaded with the shunt regulator, comprises inverter bridge $S_{\rm i1}$ and $S_{\rm i2}$, resonant inductance $L_{\rm ri}$, resonant capacitance $C_{\rm ri}$, transformer $T_{\rm ri}$ and full-wave rectifier $D_{\rm ri1}$ and $D_{\rm ri2}$. A large filter capacitor $C_{\rm oi}$, parallel with the output side, generates a constant voltage $V_{\rm oi}$. Additionally, a shunt switch $S_{\rm ji}$, which can be a mechanical switch, is placed in parallel with the input side to bypass the faulted module. During the normal condition, the switch S_{ji} is open and the semiconductor switch Q_i operates to regulate the bus voltage. While during the faulting condition, the switch S_{ji} is closed to bypass the fault module.

The modulation waveforms are depicted in Fig. 2. In the front stage SR, PWM is used to regulate the current to control the output voltage with the switching frequency $f_{s1} = 20\ kHz$ in CM. Duty cycle is fixed to zero in MM while is 1 at the bypass mdoe. In the end stage LLC resonant converter, the switching frequency is fixed to the resonant frequency 100 kHz for all modules. All switches S_{i1} $(i = 1, ..., N)$ turned ON/OFF simultaneously under full and light load conditions with the modulating waveforms.

B. Conventional Compensation-Module Based PPP

Modular PPP is a popular choice for the ISOP structure for its high efficiency. In the conventional compensation-module based PPP [41], the power of the system is divided into two parts, main power composed of several uncontrolled modules like DC transformers (DCX) and partial power including a regulated converter as voltage compensation module(CM). As shown in Fig. 3(a), the former $(N-1)$ modules operate at the fixed resonant frequency to deliver the main power taken as main modules (MM), while the rest module regulates the output voltage $V_{\rm o}$ transferring the partial power named as CM. Since the MM resonantly operate delivering the main power, high efficiency can be obtained by the PPP method. However, there are still several challenges which are expressed as follow.

1) The input voltage range is narrow. In the conventional PPP, the voltage gain of the MM is fixed to the transformer ratio n, while only the CM can adjust the input voltage ranged from 0 to rated value $nV_{\rm o}$. Thus the total input voltage $V_{\rm in,\ PPP}$ is derived as:

$$V_{\rm in,PPP} = ((N-1)n + g_{\rm CM})V_{\rm o}, \qquad (1)$$

where $g_{\rm CM}$ is the CM voltage gain. Since the module number N and transformer ratio n are constant, the input voltage range is between $(N-1)nV_{\rm o}$ and $NnV_{\rm o}$, which is unable to adjust the current-source driven MVDC input voltage from 0 to the rated value.

2) Low efficiency is obtained in the light-load conditions. Due to the series input structure, the input power of each module is proportional to the input voltage. Then the system efficiency can be given as:

$$\eta_{\rm PPP} = \frac{(N-1)n\eta_{\rm MM} + g_{\rm CM}\eta_{\rm CM}}{(N-1)n + g_{\rm CM}}, \qquad (2)$$

where $\eta_{\rm MM}$ and $\eta_{\rm CM}$ are the efficiency of MM and CM, respectively. N is usually very large, thus the

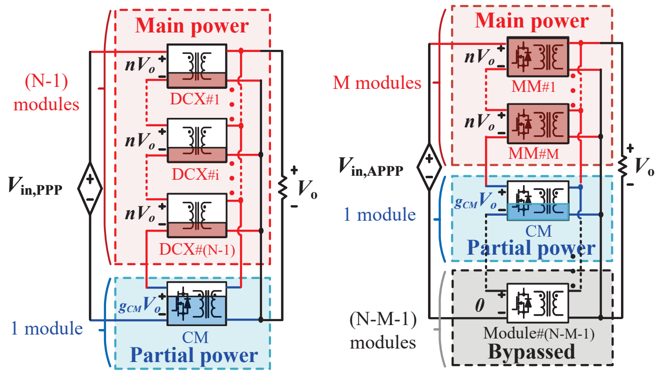

(a) Partial power processing. (b) Adaptive main-module based PPP.

Fig. 3. Structures of PPP and adaptive main-module based PPP.

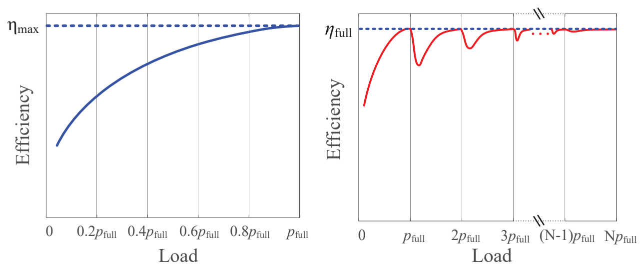

(a) Efficiency of MM based PPP system. (b) Efficiency of adaptive main-module based PPP system.

Fig. 4. Efficiency of PPP and adaptive main-module based PPP.

system efficiency is approximate equal to the single MM efficiency, as depicted in 4(a). Low efficiency is obtained in the light load conditions even the system light load power is higher than the single module full power.

3) The reliability is poor. In conventional PPP, the roles of MM and CM cannot be replaced by each other. When the single CM is failed, the system will be broken down. The system reliability is only up to the CM obtaining poor performance.

C. Proposed Adaptive Main-Module Based PPP

To address the above challenges, an adaptive main-module based PPP is proposed in this paper, as shown in Fig. 3(b). Unlike the conventional PPP with a fixed number of MM and CM, in the proposed method each module can flexibly put into or out of the system according to the load power demand. Thus the system main power can be always transmitted by several full-loaded modules acted as the MM, while the partial power is regulated by the one CM, and the rest modules are bypassed. Several advantages can be achieved by the proposed adaptive main-module based PPP method.

1) Wide input voltage range: The input voltage $V_{\mathrm{in,APPP}}$ can be calculated as

$$V_{\mathrm{in,APPP}} = ((M-1)n + g_{\mathrm{CM}})V_{\mathrm{o}}, \tag{3}$$

where M is the MM number, which is decided by

$$M = \lfloor \frac{P_{\mathrm{in}}}{P_{\mathrm{Mfull}}} \rfloor. \tag{4}$$

P_{in} is the total input power, and P_{Mfull} is full load power of each module. The MM number could adaptive vary with the real power, achieving a wide input voltage range from 0 to NnV_{o}.

2) High efficiency over wide range: Similar to the conventional PPP, the system efficiency of proposed method can be calculated as

$$\eta_{\mathrm{APPP}} = \frac{(M-1)n\eta_{\mathrm{full}} + g_{\mathrm{CM}}\eta_{\mathrm{CM}}}{(M-1)n + g_{\mathrm{CM}}}, \tag{5}$$

where η_{full} is the MM efficiency at full power p_{full}. The system efficiency of proposed method is shown in Fig. 4(b).

Obviously, when the CM power is closed to zero, the system efficiency could reach the highest value. Then there could be several peak values in the efficiency curve. Even in the light load conditions, the efficiency could be also high to the maximum efficiency value of single module, achieving high efficiency performance over wide power range. Additional, when the power is large enough, M could be far higher than 1, the system efficiency is close to η_{full}.

3) High reliability: In the proposed method, each module can automatically switch among MM, CM and bypassed modes. When any module fails, the module could be quickly bypassed. The CM module could be regulated to the full power state and switch to MM due to the power gap. And a new module could be auto switched in acted as the new CM. Thus the reliability of the proposed method is increased exponentially according to the number of modules in the system, which is far higher than the conventional PPP.

III. Control Design for Adaptive Main-Module Based PPP

To implement the proposed method, the control block diagram of the adaptive main-module based PPP is given in Fig. 5, which consists of three parts: local controller, coordinated controller and central controller. The local controller is arranged in each module regulating the module output voltage to track the reference value according to the droop V-I curve. The coordinated controller provides the droop V-I curves for each module deciding each module operating states. To address the voltage error caused by the droop control, the central controller is used to adjust the offset of each module improving the control accuracy. The flowchart of the controller actions are given in Fig. 6. The detailed implementation of the proposed method is given as follow.

A. Local Controller

According to Section I, a two-stage converter is applied in each module to transfer CC to CV. The front stage employs a SR to regulate the current to control the output voltage, in which switching frequency is 20 kHz, realizing the continuous regulation of input current achieving wide voltage range. An LLC resonant converter operating at fixed resonant frequency 100 kHz is used in the end stage to match the output voltage and isolate the load.

For the SR, the output current I_{ini} is decided by the duty cycle D_{i}, given as

$$I_{\mathrm{ini}} = -D_{\mathrm{i}}I_{\mathrm{s}} + I_{\mathrm{s}}, \tag{6}$$

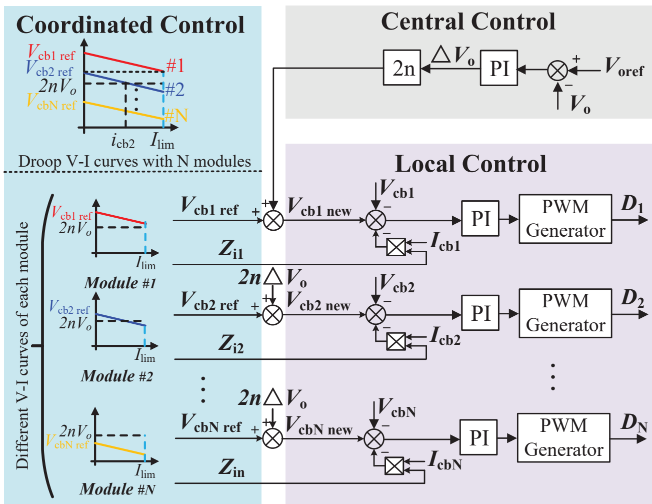

Fig. 5. The control structure of adaptive main-module based PPP.

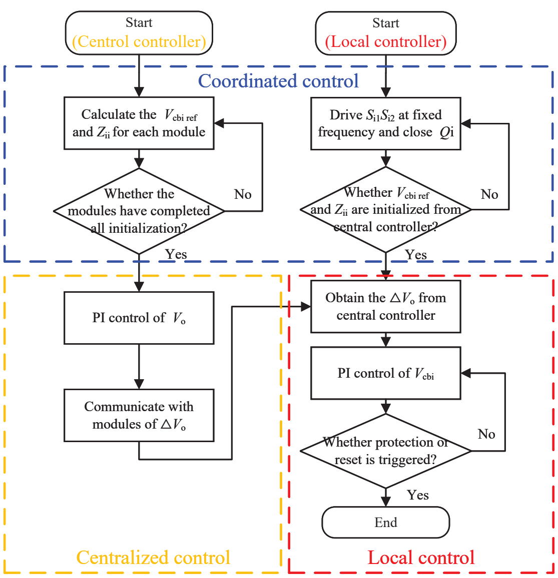

Fig. 6. Flowchart of the central controller and the module controller.

where I_s is the input current and i is the module mark number. Meanwhile, the LLC resonant converter functions as a DCX, the output voltage V_o can be derived as:

$$V_o = \frac{1}{2n} V_{cbi}, \tag{7}$$

V_{cbi} is the bus voltage of the ith module.

According to the equivalent mathematical model of LLC in the paper [44], the equivalent mathematical model of the converter is shown in Fig. 7.

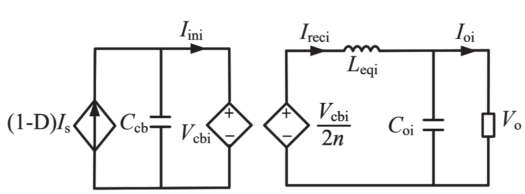

Fig. 7. Simplified equivalent circuit diagrams of the converter.

$$I_{reci} = 2nI_{ini}, \tag{8}$$

$$L_{eqi} = \frac{\pi^2}{32n^2} \frac{L_{ri}L_{mi}}{L_{ri} + L_{mi}}, \tag{9}$$

where L_{eqi} is the equivalent output inductance of the ith LLC resonant converter. L_{ri} and L_{mi} are the resonant inductance and magnetic inductance of the ith converter, respectively.

Then a state space of N modules is established, which are given as follows.

$$\begin{cases} C_{cbi}u_{cbi}s = (1-d_i)I_s - i_{ini} \\ L_{eqi}i_{reci}s = \frac{u_{cbi}}{2n} - u_o \\ C_{oi}u_o s = i_{reci} - \frac{u_o}{R_{load}} \end{cases} \tag{10}$$

Define $x = [v_{cbi}, i_{ini}, v_o]$, $u = \overline{d_i}$, $y = v_{cbi}$, $\overline{d_i} = 1 - d_i$. Then the state equations can be calculated as:

$$\begin{aligned} \dot{\mathbf{x}} &= \mathbf{Ax} + \mathbf{Bu} \\ \mathbf{y} &= \mathbf{Cx} \end{aligned} \tag{11}$$

where

$$\begin{aligned} \mathbf{A} &= \begin{bmatrix} 0 & -\frac{1}{C_{cbi}} & 0 \\ \frac{1}{4n^2 L_{eqi}} & 0 & -\frac{1}{2nL_{eqi}} \\ 0 & \frac{2n}{C_{oi}} & -\frac{1}{R_{load}C_{oi}} \end{bmatrix} \\ \mathbf{B} &= \begin{bmatrix} \frac{I_s}{C_{cbi}} \\ 0 \\ 0 \end{bmatrix} \\ \mathbf{C} &= \begin{bmatrix} 1 & 0 & 0 \end{bmatrix} \end{aligned} \tag{12}$$

then G_{du} is the transfer function from d_i to V_{cbi} given as:

$$\mathbf{G}_{du} = \frac{\mathbf{y}}{\mathbf{u}} = \mathbf{C}(\mathbf{s}I_3 - \mathbf{A})^{-1}\mathbf{B} \tag{13}$$

I_3 is a third-order unitary matrix.

To convert CC to CV, a local controller is used in each module to regulate the SR output current I_{ini} to track the output voltage, as shown in Fig. 8. Specially, in this system the common voltage between input and output sides could be large to several kV. To avoid the expensive sample costs and delays, the bus voltage V_{cbi}, instead of output voltage V_o is feed back to the controller. As shown in the figure, G_{du} is the transfer function from duty cycle to bus voltage, and G_{pii} is the PI controller.

Due to the DCX, the output voltage error could be very small in the indirect controller, which is influenced by the output impedance Z_{cbi}. Further, this error can be eliminated by the central controller.

Meanwhile, to achieve an adjustable droop curve, a virtual impedance Z_{ii} is also added in the controller. Then the output voltage V_{oi} can be derived as:

$$V_o = \frac{1}{2n} \frac{G_{pii}G_{du}}{1 + G_{pii}G_{du}} (V_{cbi\ ref} - I_{cbi}Z_{ii}), \tag{14}$$

where $V_{cbi\ ref}$ is the bus voltage reference value and I_{cbi} is the bus current. Then each module has an adjustable V-I curve.

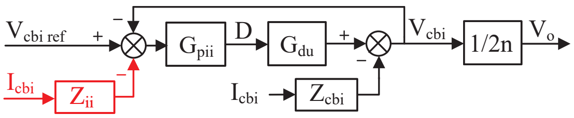

Fig. 8. The diagram of the control strategy with virtual impedance.

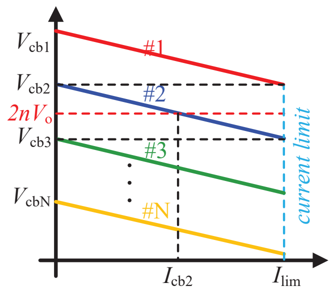

Fig. 9. The proposed different and continuous V-I curves.

B. Coordinated Controller

In the current-source driven MVDC, each module operating states are decided by its V-I features. Then the coordinated controller is given to regulate the each module V-I curve to adjust the power distribution. Unlike the traditional methods, each module has the same V-I curve sharing the same power, each module V-I curves are different and continuous arranged in the proposed method, as shown in Fig. 9. Each module operating state is decided by its V-I future and output voltage, which can be divided into three categories, as shown in follows:

1) V-I curve is above $2nV_{\mathrm{o}}$, e.g. Module 1. The duty cycle D could be adjusted to the minimum value 0 and the converter operates in current limiting state, providing the maximum current I_{lim} with clamped voltage V_{o}.
2) V-I curve is below $2nV_{\mathrm{o}}$, e.g. Module 3 to N. The duty cycle D could be adjusted to 1. Since the modules' output voltage is still below V_{o}, the rectifier could block current and stop the converter.
3) V-I curve crosses $2nV_{\mathrm{o}}$, e.g. Module 2. The duty cycles of each module are adjusted within the range of 0 – 1 to maintain the output voltage $2nV_{\mathrm{o}}$. The output current I_{cb2} is determined by the V-I features.

To achieve the continuous arranged V-I curves, design method of the adjustable V-I curves are presented.

1) Step 1: calculate the adjustable voltage range ΔV_{cb} of each module, which can be achieved from the follow equation.

$$\Delta V_{\mathrm{cb}} = \frac{2n(V_{\mathrm{o\ max}} - V_{\mathrm{o\ min}})}{N}, \tag{15}$$

where $V_{\mathrm{o\ max}}$ and $V_{\mathrm{o\ min}}$ are the allowable maximum and minimum output voltage. N is the total module number.

2) Step 2: decide the voltage range of each module. To achieve the continuous arranged V-I curves, the beginning and the end voltage of each module V-I curve should be designed one by one, which are derived as follow:

$$V_{\mathrm{cbi\ ref}} = 2nV_{\mathrm{o\ max}} - (i-1)\Delta V_{\mathrm{cb}}, \tag{16}$$

$$V_{\mathrm{cbi\ end}} = 2nV_{\mathrm{o\ max}} - i\Delta V_{\mathrm{cb}}, \tag{17}$$

where $V_{\mathrm{cbi\ ref}}$ and $V_{\mathrm{cbi\ end}}$ are the beginning and the end voltage of the ith module V-I curve.

3) Step 3: achieve the virtual impedance Z_{ii} of each module.

$$Z_{\mathrm{ii}} = \frac{V_{\mathrm{cbi\ ref}} - V_{\mathrm{cbi\ end}}}{I_{\mathrm{lim}}}. \tag{18}$$

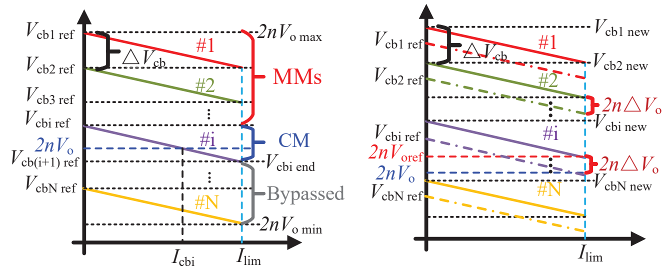

(a) Vertical adjustment of V-I curve for single module.

(b) Vertical adjustment of V-I curves for all modules.

Fig. 10. Vertical adjustment of V-I characteristic curve.

Then, the vertical adjustment of V-I curve is shown in Fig. 10(a), the module i operates at full load when the voltage $2nV_{\mathrm{o}}$ is less than $V_{\mathrm{cbi\ end}}$. The module transfers main power in current limiting state. Whereas the module i stop working when $2nV_{\mathrm{o}}$ is larger than $V_{\mathrm{cbi\ ref}}$. When $2nV_{\mathrm{o}}$ is in the range of $V_{\mathrm{cbi\ ref}}$ and $V_{\mathrm{cbi\ end}}$, module i transfers partial power, operating as a CM to stabilize the output voltage. Since the V-I curves are continuous arranged, only one module operates as CM achieving high efficiency. Specially, Module i is in full power when the output voltage is down to $V_{\mathrm{cbi\ end}}$, switching from CM to full loaded module. Otherwise, Module i is bypassed.

When $2nV_{\mathrm{o}} \in [V_{(\mathrm{cb(i+1)})\mathrm{ref}}, V_{(\mathrm{cbi})\mathrm{ref}}]$, modules 1 to $i-1$ can operate at full power, while modules $i+1$ to N remain in standby mode. The system output voltage is regulated by module i, serving as a CM when the output power P_{out} is

$$P_{out} \in [(i-1)\eta_{\mathrm{full}} P_{\mathrm{Mfull}}, i\eta_{\mathrm{full}} P_{\mathrm{Mfull}}]. \tag{19}$$

Each module can flexibly put into or out of operating according to the load power demand in the proposed method.

C. Central Controller

Due to the droop V-I curves of each module, the output voltage could vary with the load. To achieve an accurate output voltage, the central controller is used to calculate the module offset values, which can be transmitted from the central controller to each module controller to modify the output voltage error through the long delay communication, as shown in Fig. 5.

The output voltage V_{o} will be offset ΔV_{o} with the output voltage reference value V_{oref}, as shown in Fig. 10(b). Then a new bus voltage reference value $V_{(\text{cbi})\text{new}}$ is provided by the central controller, expressed as

$$V_{cbi\ new} = V_{cbi\ ref} + 2n\Delta V_{\text{o}}. \tag{20}$$

In general, the stability and dynamical performance of each module is decided by the local controller while the steady state accuracy is ensured by the long delay corrective control in the central controller.

IV. Analysis of the Proposed Adaptive Main-Module Based PPP

A. Power Features

1) Input Voltage Range: As shown in Fig. 2(a), when Q_i is ON, the module input voltage V_{ini} is zero. Otherwise, $V_{\text{ini}} = V_{\text{cbi}}$. Thus each module's input voltage V_{ini} can be expressed according to the impulse law.

$$V_{\text{ini}} = 2n(1 - D_{\text{i}})V_{\text{o}}. \tag{21}$$

V_{ini} could vary with the duty cycle D_{i} of each module's SR. Then the system input voltage of proposed method can be described as:

$$V_{\text{in,APPP}} = 2n\sum_{i=1}^{N}(1 - D_{\text{i}})V_{\text{o}}. \tag{22}$$

The power distribution of the proposed method can be drown as shown in Fig.11. The input voltage is positively correlated with the duty cycle $(1 - D_{\text{i}})$ relationship of each module, and $V_{\text{in,APPP}}$ increases with the number of operating modules. When $V_{\text{in,APPP}} \in [2n(i-1)V_{\text{o}}, 2niV_{\text{o}}]$, only the ith module's D_{i} is continuously adjustable, the other are either 1 or 0. Since the duty cycle of 5 modules are continuous arranged, the system can adjust the extreme wide voltage range from 0 to the $10nV_{\text{o}}$ in the current-source driven MVDC applications.

2) Power Distribution: The output power will be transmitted by several modules operating at MM or CM. The input power of proposed method can be described as:

$$P_{\text{in}} = V_{\text{in,APPP}}I_{\text{s}} = 2nI_{\text{s}}\sum_{i=1}^{N}(1 - D_{\text{i}})V_{\text{o}}. \tag{23}$$

The input power is proportional to the input voltage, given the input current is constant.

As shown in Fig.11, the input power keeps increasing with the rising number of $D_{\text{i}} = 0$. When $P_{\text{in}} \in [(i-1)P_{\text{Mfull}}, iP_{\text{Mfull}}]$, the power transfer consists of three modules with different operating modes: the ith module, dotted line filled frame, is CM adjusting the output voltage; the modules 1 to $i-1$, color filled frame, operate at full power; the modules $i+1$ to 5, blank frame, remain in standby mode. Each module can flexibly put into or out of the system according to the load power demand.

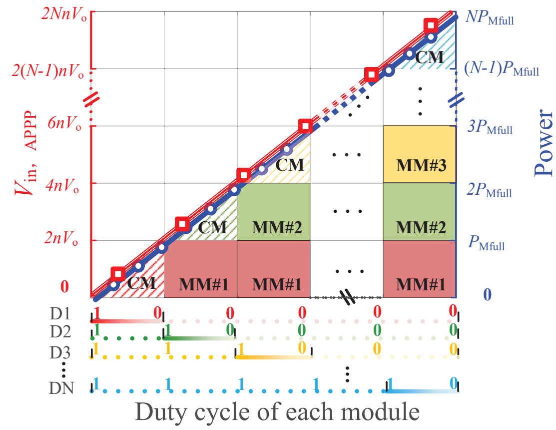

Fig. 11. Power distribution of the proposed method.

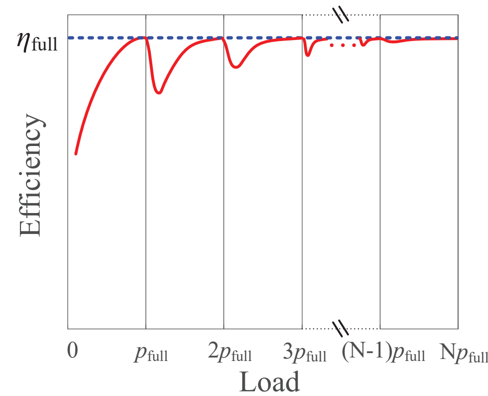

Fig. 12. Efficiency curve of proposed method.

B. Power Efficiency

The proposed two-stage converter's loss of each module is mainly caused by MOSFETs, resonant inductor, resonant capacitor, transformer and rectifier diodes. Since LLC converter works with resonant frequency leading to small power loss, the main power loss is the SR switching loss and transformer loss, which are increased as the load power rise. It is illustrated that the output efficiency of one module is approximate positively correlated with the output power [45], as shown in Fig.4(a).

According to the principle of adaptive main-module based PPP, the system efficiency is described in equation(5), which can be varied as followed:

$$\begin{aligned}\eta_{\text{APPP}} &= \eta_{\text{full}} - \frac{g_{\text{CM}}(\eta_{\text{full}} - \eta_{\text{CM}})}{(M-1)n + g_{\text{CM}}} \\ &= \eta_{\text{CM}} + \frac{(M-1)n(\eta_{\text{full}} - \eta_{\text{CM}})}{(M-1)n + g_{\text{CM}}}.\end{aligned} \tag{24}$$

By comparing the above equation, it can be derived:

$$\eta_{\text{CM}} < \eta_{\text{APPP}} < \eta_{\text{full}}. \tag{25}$$

When M is large enough, the output efficiency is closer to the full-load efficiency η_{full}. Specially, when the CM operates at the full load conditions, the system efficiency could reach the highest value. Then a new CM module appears working from light load to full load conditions as the system load

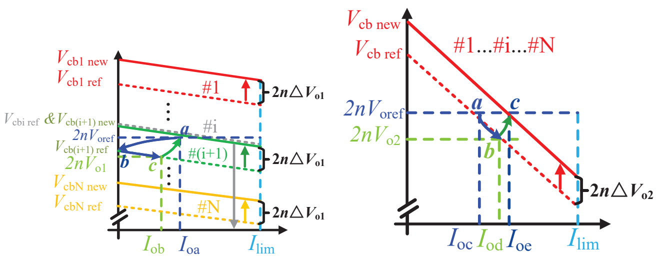

(a) Proposed method. (b) Conventional method.

Fig. 13. The operation curves of the converter under module fault conditions.

rise. Thus there could be several peak values in the efficiency curve, as shown in Fig.12. It can be also noted that the output efficiency of the proposed method is much higher than η_{CM}, resulting in high efficiency even under light load. The output efficiency is much more efficient compared conventional method.

C. Reliability Analysis

In the event of a module failure, the shunt switch S_{ji} quickly bypasses the faulty module. Then a new module could auto take over to maintain the output voltage achieving high redundancy and reliability.

The operation of the converter under module fault conditions is shown in Fig. 13. With the proposed method, the converter operates at point a as shown in Fig. 13(a). Module 1 to $i-1$ operate in current limiting state for their V-I curves are above $2nV_{oref}$. Module $i+1$ to N stop working since their voltage is below $2nV_{oref}$. Module i is regulated to control the output voltage to $2nV_{oref}$. When one module among 1 to i faults and is bypassed, output voltage could quickly fall, output current of module i could rise to the limited current. Module $i+1$ begins working at point b. Finally, module $i+1$ could work at point c with output voltage of $2nV_{o1}$. Then the central controller could increase ΔV_{o1} and the VI curves of all modules could rise. Then the output voltage could be regulated to $2nV_{oref}$ and converter operates at point a again.

In conventional method, the converter operates at point a as shown in Fig. 13(b). Since the V-I curves of all modules are the same, each module shares the same current. When one module faults and is isolated, the rest $N-1$ modules could increase the output current and work at point b with output voltage of $2nV_{o2}$. Then the central controller could increase ΔV_{o2} and the converter operates at point c with output voltage of $2nV_{oref}$.

No matter which module fails, it does not affect the normal operation of the system, and the reliability of the proposed method is greatly improved compared with the traditional method.

D. Complexity Analysis

The proposed method uses hierarchical control. The bottom local controller uses independent control for only individual module.The middle layer is pre-control and done in initialization. The top layer control is used to compensate the output voltage error, which is not sensitive to the communication delay. Thus the rising communication delay provided by the modular system could not have effects on the dynamic performance. Compared to the conventional method, the proposed method has less complexity due to the following reasons.

1) Simpler design of control parameters. During the operation of the system, only one module of the proposed method is regulated and the rest of the modules are open-loop controlled or bypassed. Whereas all the modules of the conventional method are closed-loop controlled. The proposed method has less inter-module coupling effects and less factors to be considered for parameter design.
2) Higher stability. The proposed method has only a single module being closed-loop controlled without considering the coupling relationship with the system, while the traditional method has each module being closed-loop controlled with strong coupling and a smaller stability margin interval. Meanwhile, the communication delay has a greater impact on the robustness of the parameters of the conventional method.
3) More reliable fault reconfiguration. Each module can automatically switch among MM, CM and bypassed modes, and fails of any one module will not affect the overall system characteristics. While the redundancy modules are constant in conventional. Fails of any module makes the remaining modules share the lost power, requiring additional calculations to ensure the stability of the system.

E. Controller Design

The PI parameters design method is given as follows.

1) Step 1: establish the transfer function between the duty cycle and output voltage based on the model in Section III.
2) Step 2: according to the given phase angle margin and frequency bandwidth, the PI parameters can be calculated by using the pole placement method.
3) Step 3: verify the stability. Obtain the output impedance of the input current source. Based on the Middlebrook method, the criteria of the converter input impedance can be achieved. Then the PI parameters design criteria can be obtained.
4) Step 4: Optimize the PI parameters. Using the trial-and-error method, the optimized PI parameters can be optimized after a large number of experiments.

The key parameters are mainly affected by the resonant cavity. Since the resonant frequency is high to $100\ kHz$ far larger than the controller cutoff frequency, the perturbation of the key parameters has little effect on the controller, achieving highly robustness.

V. Experimental Validation

To validate the proposed method, a current-source driven MVDC platform, as shown in Fig. 14, is built according to the parameters listed in Table II. Since the voltage stress of per switching tube is $600V$, considering twice the voltage stress,

TABLE II
SYSTEM PARAMETER

Converter parameter	Symbols	Values
SR switches	$Q_1 - Q_N$	IMW120R045M1
Half-bridge switches	$S_{11} - S_{N2}$	IMW120R045M1
SR diodes	$D_1 - D_N$	IXYS DSEP12-12A
Rectifier diodes	$D_{r11} - D_{rN2}$	IXYS DSEP12-12A
Local controller	$\setminus$	DSP28069
Central controller	$\setminus$	STM32F407
Input current	I_s	1A
Output voltage	V_o	375V
Output power	P_o	1.5kW
Single converter output power	P_{oi}	500W
SR switching frequency	f_{sb}	20kHz
Busbar voltage	V_{cb}	600V
Busbar capacitance	C_{cb}	44uF
LLC switching frequency	f_s	100kHz
resonant capacitor	C_r	22nF
resonant inductor	L_r	92uH
excitation inductance	L_m	800uH
Output filter capacitor	C_o	60uF
Local controller P parameter	P	0.01
Local controller I parameter	I	0.00005

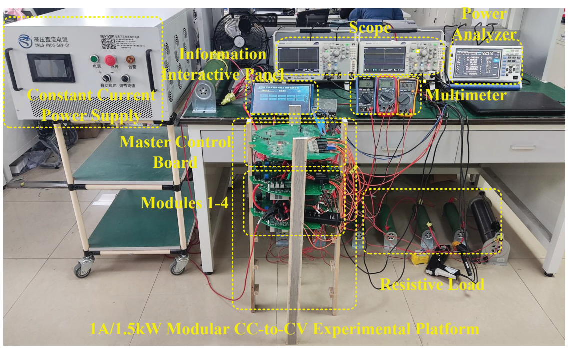

Fig. 14. Platform of current-source driven MVDC.

the MOS tube model IMW120R045M1 is used, which can withstand a maximum voltage of 1200V. Fig. 15 illustrates the top and bottom views of the single board, comprising two modules with a symmetrical structure, and the dimensions of the converter with diameter of 40 cm and height of 6 cm. The transformer's turns ratio is 0.8:1. The input current is set to 1 A, while the output voltage is maintained at 375 V. Furthermore, three modules are employed to deliver 1.5 kW, with one module serving as a redundancy.

A. Operating Waveforms of MVDC

Fig. 16 shows the waveforms of the shunt regulator circuit. v_{gs1} is the driving voltage. The bus voltage V_{bus} can be stabilized at 580V. Due to the poor dynamical performance of the current source, significant ripples are observed in the input current, although the average value is maintained at 1 A.

Fig. 17(a) and Fig. 17(b) show the waveforms of the LLC resonant converter at 30% and 80% of the rated load respectively. v_{ds1} is the drain-source voltage value of S_1, i_{r} is the resonant current, and v_{gs1} is the driving waveform of S_1. It can be noted that the converter achieves ZVS for the primary switches.

Fig. 18 shows the waveforms of no load condition, the output voltage is constant at 375 V and the output current is 0. The input voltage is approximated to be 0 due to inherent losses within the circuit.

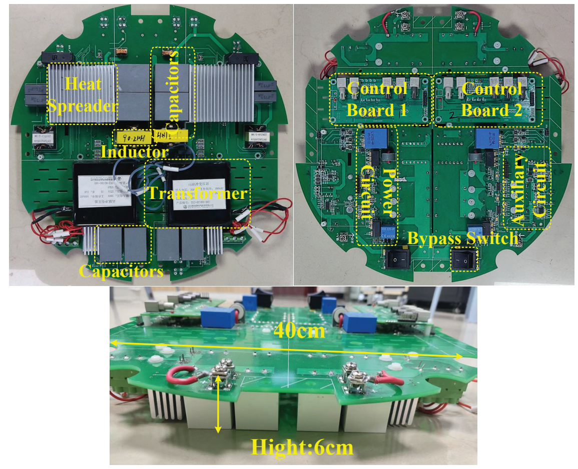

Fig. 15. Top and bottom views of a single board.

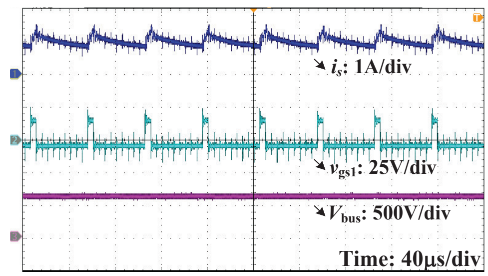

Fig. 16. Waveforms of shunt regulator.

Load switching and fault switching and experiments are conducted to verify the redundancy and dynamic performance of the proposed method.

The waveforms of a load step from 450 W to 750 W

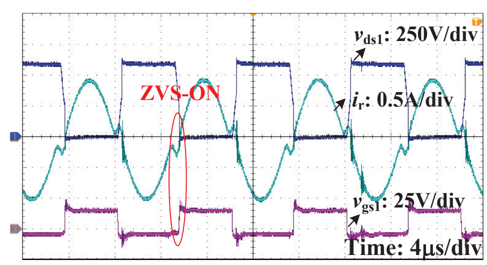

(a) 30% load.

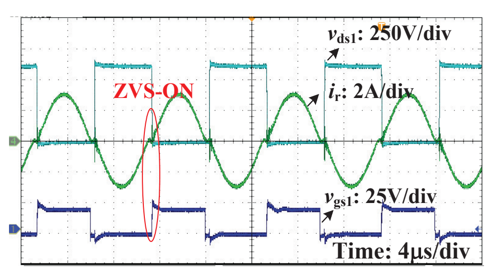

(b) 80% load.

Fig. 17. Waveforms of LLC resonant converter.

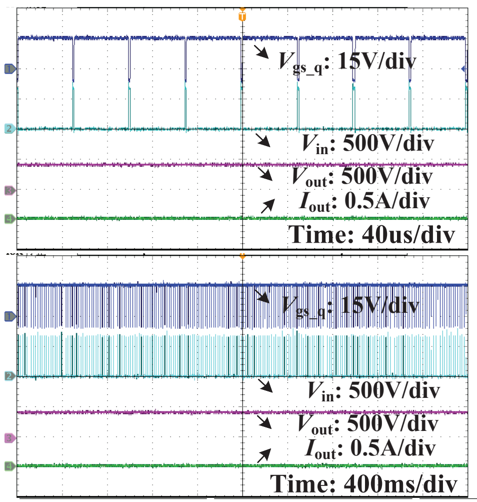

Fig. 18. Waveforms of the converter under no load conditions.

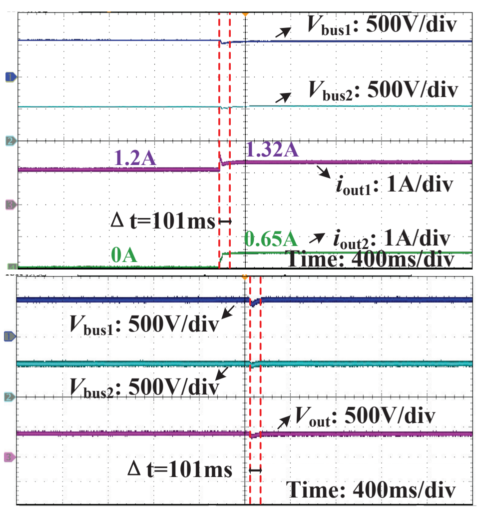

(a) Proposed method.

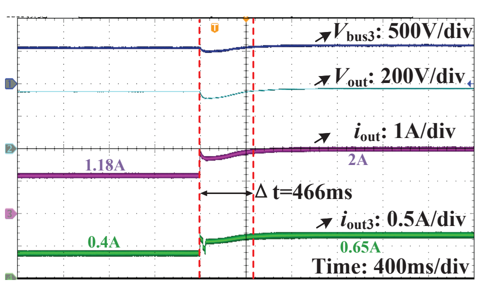

(b) Conventional balance control method.

Fig. 19. Waveforms of load step from 450 W to 750 W.

with proposed adaptive main-module based PPP method is presented in Fig. 19(a). At first, only module 1 operates with an output power of about 450 W, while module 2 and 3 are on standby. As the load increases to 750 W, module 1 is regulated to the maximum power of 500 W, and then module 2 automatically activates to provide the remaining power of 250 W. As depicted in Fig. 19(a), the output current of module 1 increases to a limited value of 1.32 A, and the output current

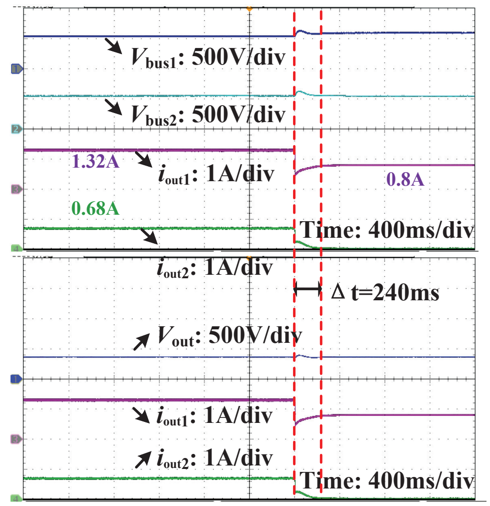

(a) Proposed method.

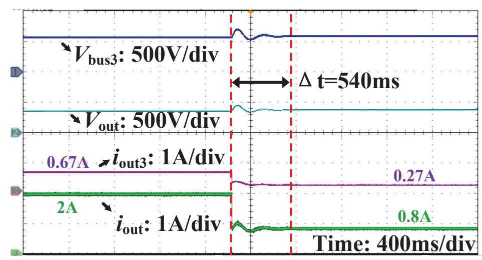

(b) Conventional balance control method.

Fig. 20. Waveforms of load decline from 750 W to 300 W.

of module 2 rises from 0 to 0.65 A. The setting time is only 101 ms.

To compare with the conventional method farily, the same PI parameters are employed. Fig. 19(b) illustrates the load step waveforms of balance control. At first, three modules output 0.4 A equally. When the load steps up, all modules increase the current to 0.65 A to maintain the output voltage. However, the setting time is prolonged, reaching 466 ms, which is slower than that of the proposed method.

The waveforms of a load decline from 750 W to 300 W with proposed adaptive main-module based PPP method is presented in Fig. 20(a). Firstly, module 1 is regulated to the maximum power of 500 W, and then module 2 activates to provide the remaining power of 250 W, while module 3 are on standby. As the load declines to 300 W, only module 1 operates with an output power of about 300 W, while module 2 and 3 are on standby. As depicted in Fig. 20(a), the output current of module 1 reduces from a limited value of 1.32 A to 0.8A, and the output current of module 2 reduces from 0.68 A to 0. The setting time is only 240 ms.

Fig. 20(b) illustrates the load decline waveforms of balance control. At first, three modules output 0.67 A equally. When the load decline, all modules reduce the current to 0.27 A to maintain the output voltage. However, the setting time is prolonged, reaching 540 ms, which is slower than that of the proposed method.

The module fault switching waveforms of the proposed method is presented in Fig. 21(a). Initially, two modules operate to generate 700 W of output power using the proposed adaptive main-module based PPP method. Module 1, which doesn't require any control, operates with minimum duty cycle to provide a maximum power of 500 W, while Module 3 remains on standby with duty cycle of 1. Module 2 is regulated to generate the remaining power of 200 W. In the event of a fault causing Module 2 to stop operation, the output voltage may drop by approximately 38 V. Then Module 3 begins working, automatically compensating for the lost power. Since the output voltage is smaller than the reference value, the central controller starts to compensate the voltage error, enabling the output voltage to return to 375 V within 124 ms. The proposed method achieves seamless and automatic fault switching.

Fig. 21(b) presents the waveforms of fault switching case using conventional balance method. Initially, three modules operate equally to generate 700 W of output power. If Module 3 stops operation due to a fault, both Module 1 and 2 can increase their output power to maintain the output voltage. However, additional balance control required will slow down the dynamic performance. The output voltage droop is approximately 45 V, and the setting time is 288 ms, both of which are slower than those achieved with the proposed method.

B. Power Features

The measured input and output voltage versus output power from $200W$ to $1500W$ of proposed method is shown in Fig.22(a). The shaded portion represents the amount of power transmitted by the module. As the delivered power P_{o} increases, the input voltage rises from 241 V to 1630 V while the output voltage keeps 375 V, achieving wide voltage ratio range.

It should be noted that since the converter is current source driven with a wide input voltage range, an inherent characteristic no matter which compared method is used, unlike conventional PPP with limited voltage range of voltage source driven. The curve of the conventional method is shown in Fig.22(b). In the proposed method, each module can flexibly put into or out of the system according to the load power demand. Whereas the number of MM and CM are fixed in the conventional methods. Each module share the same power.

C. Power Efficiency

The measured efficiency curves vs. the power are depicted in Fig. 23 and the loss breakdown of each module is given in Fig. 24. The blue and red lines indicate the efficiency curves of the conventional and proposed methods, respectively. When $P_{\text{out}} \in [0, 500W]$, only one module of the system is engaged, thus the efficiency is the same as the conventional method. When $P_{\text{out}} \in [500W, 1000W]$, two modules are put into operation, one running at full load and the other at light load. Since the light load efficiency is lower, overall output efficiency is below full load efficiency. Since all the three modules are engaged at $1200W$, which put into the same number of modules as the conventional method, the losses for both methods are close, thus efficiency is close to the same.

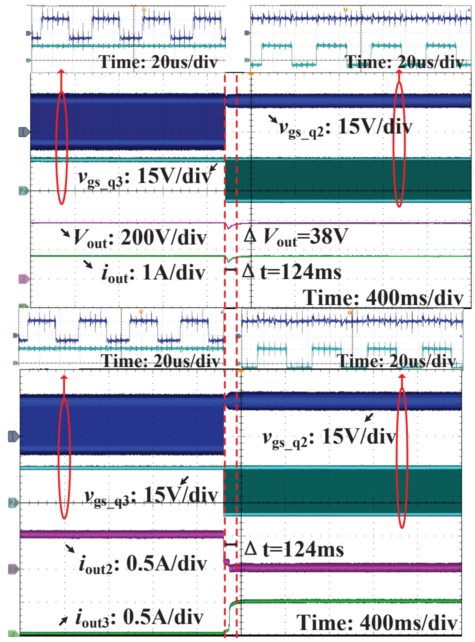

(a) Proposed method.

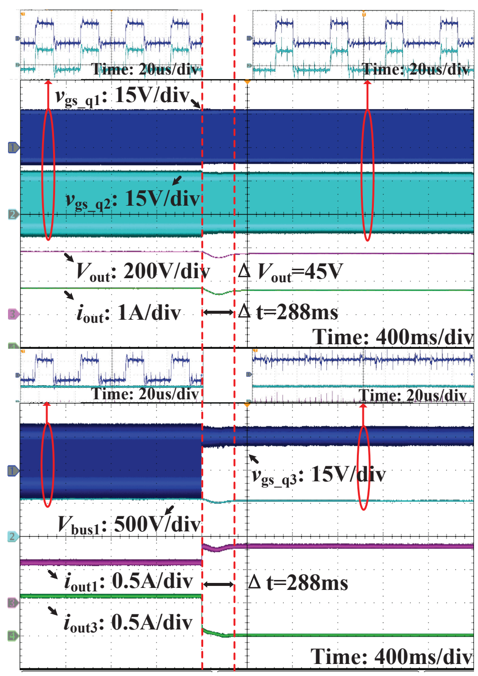

(b) Conventional balance control method.

Fig. 21. Waveforms of module fault switching case.

It can be observed that the efficiency of the proposed method increases from 83% to 92% as the load is increased from 200 W to 1500 W. This improvement is significantly higher than that achieved with conventional method, especially under light load conditions.

VI. Conclusion

This paper introduces a novel control method, named adaptive main-module based partial power processing, for a

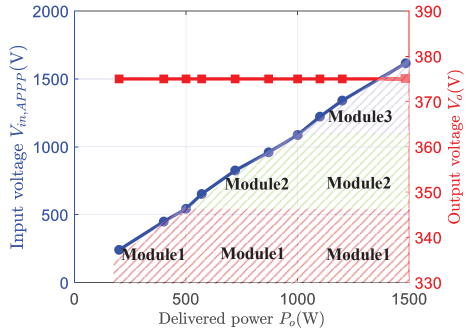

(a) Proposed method.

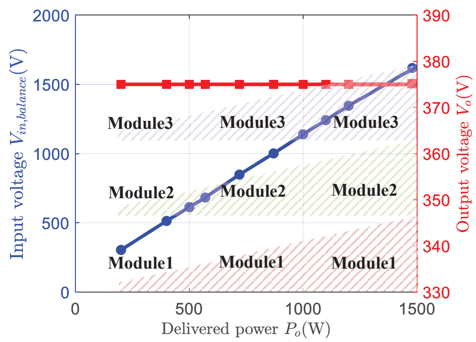

(b) Conventional balance control method.

Fig. 22. Curves of input and output voltage versus output power.

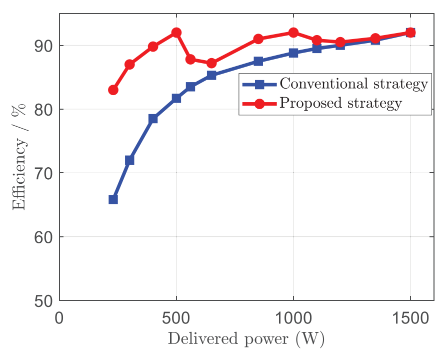

Fig. 23. Efficiency comparison between the conventional balance control and the proposed main-module based PPP.

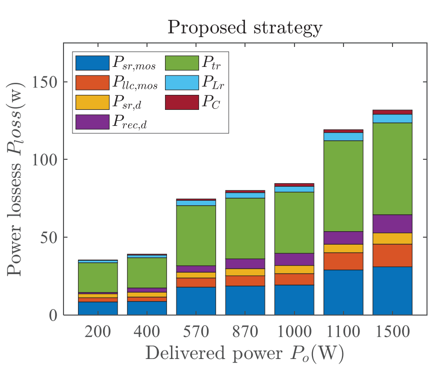

Fig. 24. Power loss breakdown of proposed method.

current-source driven modular medium voltage DC/DC converter. Unlike the conventional partial power processing with a fixed number of MM and CM, in the proposed method each module can flexibly put into or out of the system according to the load power demand. Compared conventional method, the proposed strategy has a wider range of input voltage, higher efficiency in the light load conditions and greater reliability. Experimental results demonstrate high efficiency especially under light load and greater reliability in the event of a module failure, validating the advantages of the proposed method.

References

[1] A. A. Periola and M. Sumbwanyambe, "An underwater network for mini-submarineunderwater observatory", *Proc. 2023 Int. Conf. AI, BD, Comp., DC Systs.,* pp. 1-6, 2023.

[2] C. Diouf, Veronique Quintard, Laura Ghisa, et al., "Design, characterization, and test of a versatile single-mode power-over-fiber and communication system for seafloor observatories", *IEEE J. Ocean. Eng.,* vol. 45, no. 2, pp. 656-664, Apr. 2020.

[3] K. Rajashekara, H. S. Krishnamoorthy and B. S. Naik, "Electrification of subsea systems: Requirements and challenges in power distribution and conversion", *CPSS Trans. Power Electron. Appl.,* vol. 2, no. 4, pp. 259-266, Dec. 2017.

[4] Y. Zang, Y. Chen, C. Yang, et al., "A new approach for analyzing the effect of non-ideal power supply on a constant current underwater cabled system", *Front. Inf. Technol. & Electron. Eng.,* vol. 21, no. 4, pp. 604-614, Feb. 2020.

[5] K. Asakawa, J. Kojima, J. Muramatsu, et al., "Current-to-current converter for scientific underwater cable networks", *IEEE J. Ocean. Eng.,* vol. 32, no. 3, pp. 584-592, Jul. 2007.

[6] H. NC, L. TW, H. SK, et al., "Improvement of earthquake locations with the Marine Cable Hosted Observatory (MACHO) offshore NE Taiwan", *Mar. Geophys. Res.,* vol. 35, no. 3, pp. 327-336, Mar. 2014.

[7] C. R. Barnes, M. M. R. Best, F. R. Johnson, et al. "Challenges, benefits, and opportunities in installing and operating cabled ocean observatories: Perspectives from NEPTUNE Canada", *IEEE J. Ocean. Eng.,* vol. 38, no. 1, pp. 144-157, Jan. 2013.

[8] T. Kanazawa, "Japan Trench earthquake and tsunami monitoring network of cable-linked 150 ocean bottom observatories and its impact to earth disaster science", *Proc. 2013 IEEE Int. Conf. Underw. Technol.,* pp. 1-5, 2013.

[9] K. Kawaguchi, Y. Kaneda and E. Araki, "The DONET: A real-time seafloor research infrastructure for the precise earthquake and tsunami monitoring", *Proc. 2008 MTS/IEEE Kobe OCEANS Tech. Ocean* pp. 1-4, 2008.

[10] J. -K. Choi, T. Yokobiki and K. Kawaguchi, "ROV-based automated cable-laying system: application to DONET2 installation", *IEEE J. Ocean. Eng.,* vol. 43, no. 3, pp. 665-676, Jul. 2018.

[11] Z. Duan, J. Wang, A. Yi, et al., "A load sensitive method for constant current seafloor observatory based on multi-module-stack CC/CV converter", *Proc. 5th Asia Energy Electr. Eng. Sympo.* pp. 506-511, 2023.

[12] Sa Xiao, Dengjun Li, Yanhu Chen, et al., "Modular CC/CV converter and its control strategy", *Journal of Mechanical Engineering,* vol. 56, no. 14, pp. 196-206, Jul. 2020

[13] Y. Chen, Y. Zang, C. Yang, et al., "Reconfigurable power converter for constant current underwater observatory," *Electronics*, vol. 9, no. 2, p. 307, Feb. 2020.

[14] H. Wang, T. Saha, B. Riar and R. Zane, "Design considerations for current-regulated series-resonant converters with a constant input current", *IEEE Trans. Power Electron.,* vol. 34, no. 1, pp. 141-150, Jan. 2019.

[15] T. Saha, A. C. Bagchi, H. Wang and R. A. Zane, "Bidirectional LCL-T resonant DC–DC converter for priority loads in undersea distribution networks", *IEEE Trans. Power Electron.,* vol. 37, no. 12, pp. 14874-14887, Dec. 2022.

[16] Z. Hou, D. Jiao, and J.-S. Lai, "An ultrawide range pulse width modulated LLC converter with voltage multiplier rectifiers," *IEEE Trans. Power Electron.*, vol. 40, no. 4, pp. 6216-6229, Apr. 2025.

[17] Y. Wang, F. Wang, F. Zhuo, et al., "Synchronous rectification and parameter design based on accurate time-domain model for asymmetrical CLLC resonant converter," *IEEE Trans. Transp. Electrific.*, vol. 11, no. 1, pp. 4681-4697, Feb. 2025.

[18] E. Altamiranda and E. Colina, “A system of systems digital twin to support life time management and life extension of subsea production systems,” *Proc. OCEANS*, pp. 1-9, 2019.
[19] V. Vorperian, “Synthesis of medium voltage Dc-to-Dc converters from low-voltage, high frequency PWM switching converters”, *IEEE Trans. Power Electron.,* vol. 22, no. 5, pp. 1619-1635, Sep. 2007.
[20] P. Fischer, H. Brix, B. Baschek, et al., “Operating cabled underwater observatories in rough shelf-sea environments: A technological challenge”, *Proc. Front. Mar. Sci.,* pp. 1-20, 2020.
[21] M. Uno and K. Hasegawa, “Modular equalization system based on star-connected phase-shift switched capacitor converters with inherent constant current characteristics for electric double-layer capacitor modules”, *IEEE Trans. Power Electron.,* vol. 35, no. 10, pp. 10271-10284, Oct. 2020.
[22] Zheng, Shaoduo and Feng Lyu, “Compact medium voltage DC/DC converter using series-connected power devices,” *Electronics*, vol. 9, no. 6, p. 1024,Jun. 2020.
[23] J. Duan, D. Zhang, L. Wang, et al., “A building block method for input-series-connected DC/DC converters”, *IEEE Trans. Power Electron.,* vol. 36, no. 3, pp. 3063-3077, Mar. 2021.
[24] Q. Liu, Y. Wang, S. Wang, et al., “Voltage regulation strategy for DC distribution networks based on coordination of centralized control and adaptive droop control,” *IEEE Trans. Power Deliv.*, vol. 37, no. 5, pp. 3730-3739, Oct. 2022.
[25] C. Luo and S. Huang, ”Novel voltage balancing control strategy for dual-active-bridge input-series-output-parallel DC-DC converters,” *IEEE Access*, vol. 8, pp. 103114-103123, Jun. 2020.
[26] W. Chen and G. Wang, ”Decentralized voltage-sharing control strategy for fully modular input-series–output-series system with improved voltage regulation”, *IEEE Trans. Ind. Electron.,* vol. 62, no. 5, pp. 2777-2787, May. 2015.
[27] Y. Zeng, J. Pou, C.J. Sun, et al., ”Autonomous input voltage sharing control and triple phase shift modulation method for ISOP-DAB converter in DC microgrid: A multiagent deep reinforcement learning-based method”, *IEEE Trans. Power Electron.,* vol. 38, no. 3, pp. 2985-3000, Mar. 2023.
[28] A. Bach, J. Mathé, B. J. Mortimer, et al., ”Impedance-based modeling and stability analysis of the input-series output-parallel DAB3 converter with decentralized control”, *Proc. IEEE 24th Wksp. Control Model. Power Electron.,* pp. 1-8, 2023.
[29] L. Zhu, C. Li, H. Yang, et al., “Buck-boost type high step-down low power modular converter for medium voltage DC systems,” *IEEE Trans. Power Electron.*, vol. 38, no. 1, pp. 634-646, Jan. 2023.
[30] J. Liu, S. Zhong, J. Zhang, Y. Ai, N. Zhao and J. Yang, “Aux power supply for medium-/high-voltage and high-power solid-state,” *IEEE Trans. Power Electron.*, vol. 35, no. 5, pp. 4791-4803, May. 2020.
[31] S. Chowdhury, M. N. B. Shaheed, and Y. Sozer, “State-of-charge balancing control for modular battery system with output DC bus regulation,” *IEEE Trans. Transp. Electrif.*, vol. 7, no. 4, pp. 2181–2193, Dec. 2021.
[32] L. Qin, T. Wu, Y. Guan, et al., “Decoupling control strategy for input-series-output-parallel dual active bridge converter based on linear active disturbance rejection control,” *IEEE Trans. Ind. Appl.*, pp. 1-14, Feb. 2025.
[33] J. Anzola, I. Aizpuru, A A Romero, et al., ”Review of architectures based on partial power processing for DC-DC applications”, *IEEE Access,* vol. 8, pp. 103405-103418, Jun. 2020.
[34] N. Hassanpour, A. Chub, A. Blinov, et al., ”Soft-switching bidirectional step-up/down partial power converter with reduced components stress”, *IEEE Trans. Power Electron.,* vol. 38, no. 11, pp. 14166-14177, Nov. 2023.
[35] M. Wang, S Pan, X Zha, et al., ”Hybrid control strategy for an integrated DAB–LLC–DCX DC–DC converter to achieve full power range zero voltage switching”, *IEEE Trans. Power Electron.,* vol. 36, no. 12, pp. 14383-14397, Dec. 2021.
[36] Q. Yu, W. Xiong, Z. Yan, et al., ”Efficiency improvement and ripple suppression method based on partial power processing for wireless power transfer system”, *IEEE Trans. Power Electron.,* vol. 38, no. 10, pp. 13181-13193, Oct. 2023.
[37] W. Xiong, Z. Yan, D. Tang, et al., ”A hybrid topology ipt system with partial power processing for CC-CV charging”, *IEEE Trans. Power Electron.,* vol. 39, no. 1, pp. 1701-1712, Jan. 2024.
[38] N. Hou, L. Ding, P. Gunawardena, et al., ”A partial power processing structure embedding renewable energy source and energy storage element for islanded DC microgrid”, *IEEE Trans. Power Electron.,* vol. 38, no. 3, pp. 4027-4039, Mar. 2023.
[39] C. Sun, S. Wang, J. Pou, et al., “Asymmetrical-bidirectional input-series–output-parallel modular DC–DC converter in DC distribution grids with renewables,” *IEEE Trans. Power Electron.*, vol. 39, no. 4, pp. 3943-3949, April 2024.
[40] Y. Sun, Z. Gao, C. Fu, et al., ”A hybrid modular DC solid-state transformer combining high efficiency and control flexibility”, *IEEE Trans. Power Electron.,* vol. 35, no. 4, pp. 3434-3449, Apr. 2020.
[41] J. Yao, W. Chen, C. Xue, et al., ”An ISOP hybrid DC transformer combining multiple SRCs and DAB converters to interconnect MVDC and LVDC distribution networks”, *IEEE Trans. Power Electron.,* vol. 35, no. 11, pp. 11442-11452, Nov. 2020.
[42] R. Guan, Z He, Q Wei, et al., ”A high step-down partial power processing switched-capacitor converter for wide input voltage range medium voltage DC applications”, *IEEE Trans. Power Electron.,* vol. 38, no. 10, pp. 12265-12277, Oct. 2023.
[43] R. Wei and Y. R. Li, ”Optimized design and fast-dynamic control for ISOP-connected hybrid CLLC-DAB system with partial power processing property”, *IEEE Trans. Power Electron.,* vol. 39, no. 7, pp. 8844-8857, July. 2024.
[44] Z. Fang, J. Wang, R. Liu, et. al.,“Energy feedback control of light-load voltage regulation for LLC resonant converter,” *IEEE Trans. Power Electron,* vol. 34, no. 5, pp. 4807 - 4819, May. 2019.
[45] V. K. Goyal and A. Shukla, ”Two-stage hybrid isolated DC–DC boost converter for high power and wide input voltage range applications”, *IEEE Trans. Ind. Electron.,* vol. 69, no. 7, pp. 6751-6763, July. 2022.

Zhijian Fang (Member, IEEE) received the B.S. and Ph. D degree in electrical engineering and automation from Huazhong University of Science and Technology, Wuhan, China in 2010 and 2015, respectively.

From 2015 to 2018, he is a post-doctoral research fellow with the school of electrical engineering, Wuhan University, Wuhan, P. R. China. From Feb. 2016 to Jan. 2017, he was a post-doctoral research fellow with department of electrical and computer engineering, Ryerson University, Toronto, Canada. Since 2019, he is a Professor with the School of Automatic, China University of Geosciences (Wuhan). His research interests include high performance DC/DC converter, battery charger and renewable energy applications, and wireless power transfer.

Chi Zhang received the B.S. degree in automation in 2023 from the China University of Geosciences, Wuhan, China, where he is currently working toward the M.S. degree in electronic information.

His research focuses on the DC/DC converter and its control method.

Jinbo Zhao was born in Hubei, China in 1988. He received a Ph.D. degree in School of Electrical and Electronic Engineering from Huazhong University of Science and Technology in 2016. He has been working in Wuhan Maritime Communication Research Institution since 2016.

His research interests include high-power amplification and underwater remote power supply.

Han Fu received the B.S. and Ph.D. degrees in electrical engineering from Huazhong University of Science and Technology, Wuhan, China, in 2015 and 2023. He is currently working with the School of Electrical and Electronic Information Engineering, Hubei Polytechnic University (HBPU).

His research interests include modeling and control of converter, and power system with high proportion of renewable energy.

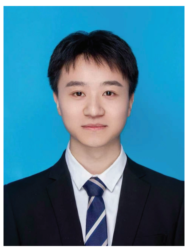

Chunyu Ye received the B.S. degree in automation in 2020 from the China University of Geosciences, Wuhan, China, where he is currently working toward the M.S. degree in electronic information.

His research focuses on power electronic converters.

Zhicong Huang (Senior Member, IEEE) received the B.Eng. degree in electrical engineering and automation and the M.Eng. degree in mechanical and electronic engineering from the Huazhong University of Science and Technology, Wuhan, China, in 2010 and 2013, respectively, and the Ph.D. degree in power electronics from The Hong Kong Polytechnic University, Hong Kong, in 2018.

In 2019, he was a Postdoctoral Fellow under the UM Macao Talent Program with the State Key Laboratory of Analog and Mixed-Signal VLSI, Macau, China. Since 2020, he has been an Associate Professor with the Shien-Ming Wu School of Intelligent Engineering, South China University of Technology, Guangzhou, China. His research interests include wireless power transfer, resonant power conversion, large-scale renewable power generation, artificial intelligence for power electronics, and wave energy converters.

Dr. Huang servers as an Associate Editor for IEEE Transactions on Consumer Electronics. He received the Outstanding Reviewer Award for IEEE Transactions on Power Electronics in 2024 and 2021, the Star Reviewer Award for IEEE Journal on Emerging and Selected Topics in Power Electronics in 2024 and 2023, and the Best Reviewer for IEEE Journal on Emerging and Selected Topics in Circuits and Systems in 2023.